Geometric effect on cooling power and performance of an integrated thermoelectric generation-cooling system

Wei-Hsin Chen [a],[*], Chien-Chang Wang [b], Chen-I Hung [b]

[a] *Department of Aeronautics and Astronautics, National Cheng Kung University, Tainan 701, Taiwan, ROC*
[b] *Department of Mechanical Engineering, National Cheng Kung University, Tainan 701, Taiwan, ROC*

ARTICLE INFO

ABSTRACT

Geometric design of an integrated thermoelectric generation-cooling system is performed numerically using a finite element method. In the system, a thermoelectric cooler (TEC) is powered directly by a thermoelectric generator (TEG). Two different boundary conditions in association with the effects of contact resistance and heat convection on system performance are taken into account. The results suggest that the characteristics of system performance under varying TEG length are significantly different from those under altering TEC length. When the TEG length is changed, the entire behavior of system performance depends highly on the boundary conditions. On the other hand, the maximum distributions of cooling power and coefficient of performance (COP) are exhibited when the TEC length is altered, whether the hot surface of TEG is given by a fixed temperature or heat transfer rate. The system performance will be reduced once the contact resistance and heat convection are considered. When the lengths of TEG and TEC vary, the maximum reduction percentages of system performance are 12.45% and 18.67%, respectively. The numerical predictions have provided a useful insight into the design of integrated TEG–TEC systems.

1. Introduction

In recent years, the problems of global warming and air pollution have greatly stimulated the development of green energy technologies. In these technologies, thermoelectric devices are receiving a great deal of attention duo to their numerous attractive merits. For example, they are compact and environmentally friendly, and can be operated easily with long life and low maintenance cost [1,2]. According to thermoelectric effects, thermoelectric devices have two different operating modes. One is the generation mode using thermoelectric generators (TEGs) to directly convert thermal energy into electrical energy [3]. The energy source of TEGs can come from waste heat which is extensively available in industry [4,5]. The other is the cooling mode whereby thermoelectric coolers (TECs) can cause a temperature difference for cooling applications by inputting electrical energy [6]. The development of TEG and TEC has been considered as a low-carbon and green energy technology, and they have been successfully applied in military, aerospace, and industry [7].

In general, TEGs and TECs are individually utilized for practical applications, such as waste heat recovery [8,9] and ceiling cooling

system [10]. Recently, an integrated TEG–TEC system has been proposed by Chen et al. [11]. In their integrated system, TECs were driven by TEGs so that no additional electrical power source was required for the TECs. They provided the optimal number ratios between the TEGs and the TECs under various operating conditions through an analytical analysis. Later, several studies also investigated the integrated systems. For example, Khattab and Shenawy [12] constructed an experimental system and successfully used solar TEGs to drive a TEC all year round. Meng et al. [13] used an analytical method to analyze the performance of a thermoelectric heat pump driven by a TEG. They found that the heat source temperature of the TEG had a greater effect on heating load than on the coefficient of performance (COP). On the contrary, the heat sink temperature of the thermoelectric heat pump had a more significant effect on the COP than on the heating load. Meng et al. [14] also adopted another analytical method to investigate the influence of physical dimensions of thermoelectric elements on the performance of an integrated TEG–TEC system. Their results indicated that performance improvements could be achieved by optimizing the physical dimensions of thermoelectric elements.

Geometric design is a crucial issue in optimizing performance of a thermoelectric system. For a given thermoelectric module, the geometrical optimization of the thermoelectric element is a feasible way to maximize its performance or efficiency [15]. Regarding

Nomenclature

A	area (mm^2)
A_c	cross-sectional area of the collector (mm^2)
C_g	concentration ratio of solar thermoelectric generator
COP	coefficient of performance of the integrated system
$\underline{D}$	depth of thermoelectric element (mm)
$\underline{E}$	electric field intensity vector (V m^{-1})
h	convection heat transfer coefficient (W m^{-2} K^{-1})
I	electric current (A)
$\underline{I}^L$	electric current load vector (A)
$\underline{J}$	electric current density vector (A m^{-2})
K^{TT}	thermal stiffness matrix
$K^{\varphi T}$	Seebeck stiffness matrix
$K^{\varphi\varphi}$	electric stiffness matrix
k	thermal conductivity (W m^{-1} K^{-1})
L	length of thermoelectric element (mm)
N	element shape function
q''	heat flux (W m^{-2})
q_s	solar irradiance (W m^{-2})
Q	heat transfer rate (W)
Q_{in}	input energy of solar thermoelectric generator (W)
Q_{TE}	input energy per thermoelectric couple (W)
Q^L	thermal load vector (W)
R	electrical resistance (Ω)
T	temperature (°C)

T_e	vector of nodal temperatures (°C)
T_∞	environment temperature (°C)
W	width of thermoelectric element (mm)

Greek letters

α	Seebeck coefficient (V K^{-1})
η_a	absorptivity of the collector coating
η_{opt}	optical efficiency of the Fresnel lens
ρ	electrical resistivity (Ω m)
ρ_{con}	electrical contact resistivity (Ω m^{-2})
ϕ	electric scalar potential (V)
φ_e	vector of nodal electric potentials (V)

Subscripts

C	thermoelectric cooler
conv	heat convection between the thermoelectric elements and the environment
G	thermoelectric generator
H	hot side
L	cold side
n	N-type thermoelectric element
p	P-type thermoelectric element

the generation mode, Jang et al. [16] analyzed the geometric effect of thermoelectric elements on micro-TEG performance by means of a finite element method. Their results showed that there was an optimal length of thermoelectric elements to achieve the highest power. Additionally, a higher efficiency could be obtained with a greater length of thermoelectric element. For the cooling mode, Lee and Kim [17] used a numerical method to investigate the cooling performance of a micro-TEC. They reported that the cooling rate increased and the maximum COP decreased when the thickness of the thermoelectric element decreased.

As far as the practical thermoelectric system is concerned, in fact, there exists an undesired effect of electrical contact resistance contributed from both interfaces and interconnects [18]. Min and Rowe [19] reported that the effect of contact resistance on the COP of a TEC became significant when the length of thermoelectric element was relatively short. Another unfavorable effect regarding geometry is heat loss to the environment from TEG surfaces. The effect of heat loss from thermoelectric elements to the ambient environment on TEG performance has been explored in recent research. For instance, a TEG system combined with parallel-plate heat exchangers was constructed by Niu et al. [20] where a hot fluid and a cold fluid passed through the hot side and the cold side of the TEG, respectively. Their experimental results indicated that heat loss from the TEG to the environment increased markedly when the inlet fluid temperature at the hot side was lifted. The theoretical analysis of Xiao et al. [21] revealed that the existence of heat loss caused a large exergy loss in a TEG system and this effect should be taken into account in the analysis. However, the geometric design of the thermoelectric system was not considered in their study.

From the review of the above literature, it is evident that specifying optimal geometric design parameters may be a promising method of improving or maximizing the performance of thermoelectric systems. However, to the authors' knowledge, very little research has been performed on the geometric design of thermoelectric systems under the effects of heat loss and electrical contact resistance, especially in an integrated TEG–TEC system. In order to provide a useful insight into the importance of geometric design for improving the performance of an integrated TEG–TEC system,

a numerical method is developed to model an integrated system and predict the performance of the system. The effects of heat loss and electrical contact resistance on the performance are taken into account. The effects of two different boundary conditions due to altered operating conditions are also considered.

2. Methodology

2.1. Physical model and assumptions

A schematic of the integrated system for study is shown in Fig. 1a where a TEC and a TEG are included in the system. In the system, the TEG absorbs heat $Q_{H,G}$ from the heat source at the hot side and liberates heat $Q_{L,G}$ to the heat sink at the cold side, thereby generating electric current through the Seebeck effect [22]. Then, the current is directly used to power the TEC, which absorbs heat $Q_{L,C}$ from the refrigerated object at the cold side and dissipates heat $Q_{H,C}$ to the heat sink at the hot side based on the Peltier effect [23]. In order to investigate the influence of heat loss on the performance of the integrated system, a heat convection process between the thermoelectric elements and its environment is taken into account. The radiation heat transfer is relatively small at low-temperature conditions [21], so it is neglected in this study. In Fig. 1a, $Q_{conv,G}$ and $Q_{conv,C}$ denote the convective heat flow rates along the lateral surfaces of the TEG and the TEC, respectively. For the sake of simplicity, the following assumptions are adopted.

(a) The integrated system is in steady-state.
(b) An identical model is used for the TEC and the TEG; therefore, they have the same configurations and material properties, except for the Seebeck coefficients which are positive and negative in the p-type and n-type elements, respectively.
(c) Material properties of the thermoelectric elements are temperature-dependent.
(d) The thermoelectric elements are connected electrically in series and thermally in parallel.
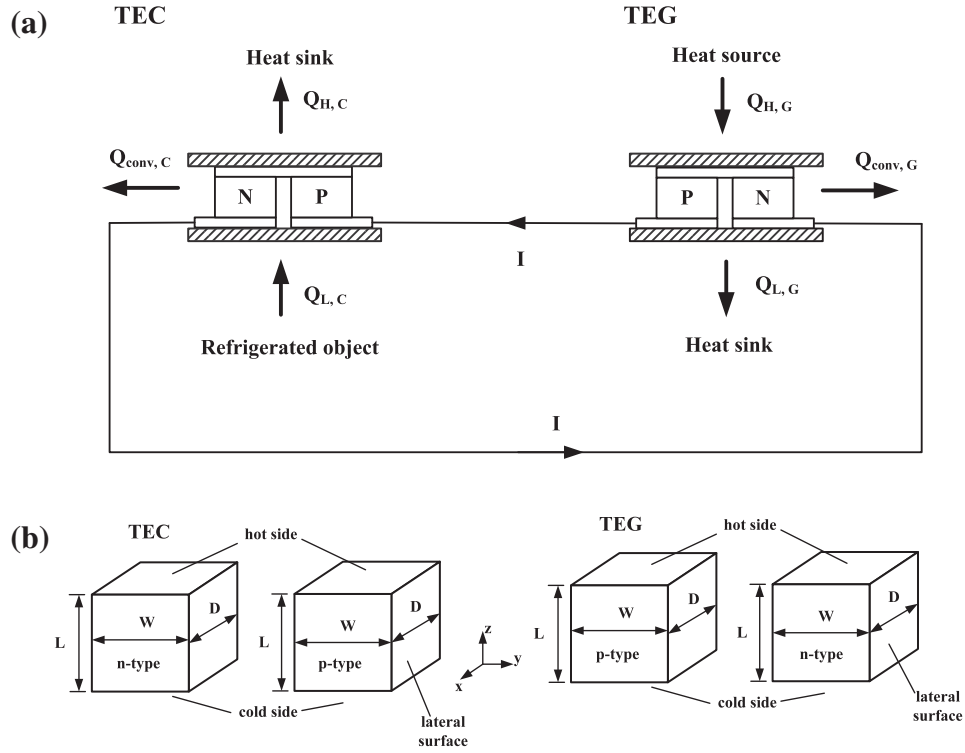
Fig. 1. Schematics of (a) the integrated TEG–TEC system for investigation and (b) thermoelectric element geometry.

(e) The contact resistivity is assumed to be constant.
(f) In the TEG or the TEC, only one thermoelectric pair, namely, a p-type element and an n-type element, are considered.

Accordingly, the computational geometries of the TEG and TEC are shown in Fig. 1b. Each thermoelectric element is specified by its depth D, width W, and length L. The lateral surfaces considering convective heat transfer exclude the hot-side and cold-side surfaces.

2.2. Governing equations

For a steady-state thermoelectric model, the governing equations include the thermal and electrical fields to describe the thermoelectric effects and they are written as [24,25]

$$\nabla \cdot (\alpha T \vec{J}) - \nabla \cdot (k \nabla T) = \vec{J} \cdot \vec{E} \tag{1}$$

$$\nabla \cdot \left(\frac{1}{\rho} \vec{E}\right) - \nabla \cdot \left(\frac{\alpha}{\rho} \nabla T\right) = 0 \tag{2}$$

where T and $\vec{J}$ represent the absolute temperature and electric current density vector, respectively; α, k, and ρ are the Seebeck coefficient, thermal conductivity, and electrical resistivity of a thermoelectric element, respectively. $\vec{E}$ is the electric field and it can be derived from electric scalar potential ϕ ($\vec{E} = -\nabla \phi$). More detailed derivations of the governing equations can be found in a previous study [25] in which a TEG system has been successfully modeled by the numerical method.

2.3. Boundary conditions

The boundary conditions are made up of three different surfaces, including hot-side surfaces, cold-side surfaces, and lateral surfaces. The hot-side and cold-side surfaces of the TEC and TEG elements are treated by Dirichlet conditions; that is, these surfaces'

temperatures are fixed. Another case with Neumann conditions for the hot-side surfaces of the TEG elements are considered for comparison. In this case, a heat transfer rate is given at the hot-side surfaces of the TEG elements. The lateral surfaces of all the thermoelectric elements are exposed to the environment along with convective heat transfer as mentioned earlier. Therefore, a uniform convective heat transfer coefficient h_{conv} is invoked at the lateral surfaces. Detailed boundary conditions are summarized in Table 1.

2.4. Numerical method and system performance

The governing equations are solved by means of the commercial software ANSYS v12.0.1 in which a finite element scheme based on the Galerkin method is used to discretize the governing equations [26]. Specifically, the physical scales of temperature T and electric scalar potential ϕ over a computational domain are approached by the finite-element method by the following equations [27]

$$T = [N]\{T_e\} \tag{3}$$

$$\phi = [N]\{\varphi_e\} \tag{4}$$

where T_e, φ_e, and N are the vector of nodal temperature, the vector of nodal electrical potentials, and the element shape function, respectively. By integrating Eqs. (1) and (2) based on the Galerkin

Table 1
A list of adopted boundary conditions.

Surface	TEC	TEG
Hot side	Dirichlet condition: $T = T_{H,C}$	Case1: Dirichlet condition: $T = T_{H,G}$ Case2: Neumann condition: $-\int k\nabla T dA = q''A = Q_{H,G}$
Cold side	Dirichlet condition: $T = T_{L,C}$	Dirichlet condition: $T = T_{L,G}$
Lateral side	Convection condition: $-k\nabla T = h_{conv}(T - T_\infty)$	Convection condition: $-k\nabla T = h_{conv}(T - T_\infty)$

method, the differential equations can be rewritten as algebraic equations [27]

$$\begin{bmatrix} K^{TT} & 0 \\ K^{\varphi T} & K^{\varphi\varphi} \end{bmatrix} \begin{Bmatrix} T_e \\ \varphi_e \end{Bmatrix} = \begin{Bmatrix} Q^L \\ I^L \end{Bmatrix} \tag{5}$$

where K^{TT}, $K^{\varphi\varphi}$, and $K^{\varphi T}$ are the thermal stiffness matrix, electric stiffness matrix, and Seebeck stiffness matrix, respectively, and they are defined as $K^{TT} = \int_v \nabla N \cdot [k] \cdot \nabla N dV$, $K^{\varphi\varphi} = \int_v \nabla N \cdot \left[\frac{1}{\rho}\right] \cdot \nabla N dV$, and $K^{\varphi T} = \int_v \nabla N \cdot \left[\frac{1}{\rho}\right] \cdot [\alpha] \cdot \nabla N dV$. Q^L and I^L in Eq. (5) are the thermal load vector and the electric current load vector, respectively. The three matrices and two load vectors are obtained by the numerical integration over the element volume. Four thermoelectric elements are considered in the numerical model, as shown in Fig. 1b. The orthogonal grid system is used for the thermoelectric elements. The test of grid system reveals that each element consisting of 5850 numerical cells satisfies the requirement of grid independence; this number of cells is thus adopted for simulations. In the calculation, the iterations are terminated as the residuals of all the equations reach the convergence criteria of relative errors less than 10^{-6}. After the numerical iterations are implemented, the temperatures (T_e) and electric potentials (ϕ_e) at each node of the numerical cells are obtained.

In the integrated system, two indices are employed to evaluate the performance of the system. One is the cooling power $Q_{L,C}$ which represents the heat pumped capacity of the TEC from the refrigerated object. The other is the COP of the system and it is expressed as [11,14]
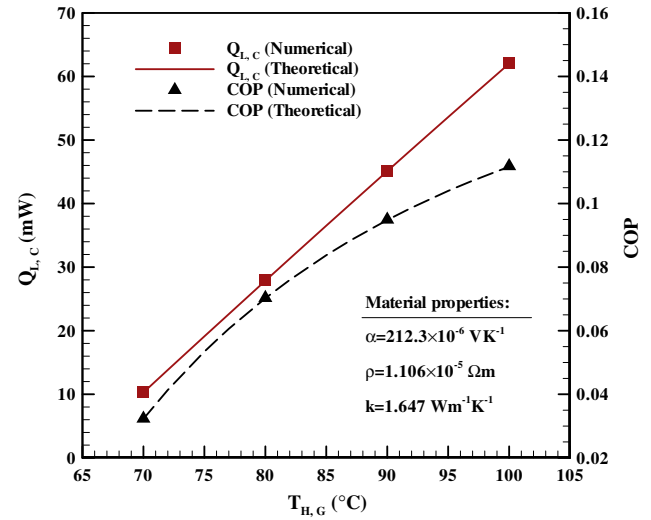
$$COP = \frac{Q_{L,C}}{Q_{H,G}} \tag{6}$$

COP means the percentage of input energy (i.e. $Q_{H,G}$) gained for cooling power by the system. The thermoelectric module TEC1-12708 presented by Maneewan and Chindaruksa [28] was chosen as the geometric design of the TEC and the TEG in this study, as given in Table 2. The temperature-dependent material properties of the thermoelectric elements, such as thermal conductivity, Seebeck coefficient, and electrical resistivity, reported by Meng et al. [29] were adopted and listed in Table 2. The material is a commercially available material produced by Melcor; however, detailed components in the material were not illustrated, perhaps due to the commercial know-how involved.

In reviewing past studies, very little experimental literature and available data have been published on the integrated system, Therefore, theoretical solutions were employed to validate numerical predictions in some studies [30–33]. Similarly, the present model is validated by comparing with the analysis of Khattab and Shenawy [12]. Their method was conducted based on one-dimensional (1-D) geometry and the assumption of ignoring heat convection between the thermoelectric elements and their environment; the formulas are given by:

$$Q_{H,G} = \alpha_G I T_{L,G} + 0.5 I^2 R_G + K_G(T_{H,G} - T_{L,G}) \tag{7}$$

Fig. 2. A comparison of one-dimensional system performance between numerical simulation and theoretical prediction.

$$Q_{L,C} = \alpha_C I T_{L,C} - 0.5 I^2 R_C - K_C(T_{H,C} - T_{L,C}) \tag{8}$$

$$I = \frac{\alpha_G(T_{H,G} - T_{L,G}) - \alpha_C(T_{H,C} - T_{L,C})}{R_G + R_C} \tag{9}$$

where α_G and α_C are the Seebeck coefficient of the TEG and TEC, respectively; R_G and R_C represent the resistance of the TEG and of the TEC, respectively; K_G and K_C are the thermal conductance of the TEG and of the TEC, respectively. The assumptions of $\alpha_G = \alpha_C = (\alpha_p - \alpha_n)$, $R_G = R_C = \frac{\rho_p L_p}{A_p} + \frac{\rho_n L_n}{A_n}$, and $K_G = K_C = \frac{k_p A_p}{L_p} + \frac{k_n A_n}{L_n}$ are considered. Therefore, the theoretical COP can be obtained from COP = $Q_{L,C}/Q_{H,G}$. By virtue of the limitation of 1-D approach, the constant material properties at T = 300 K were used and the contact resistivity ρ_{con} was set to be 1×10^{-10} Ω m^{-2} [34]. The numerical and theoretical results along with $T_{L,G}$ = 25 °C, $T_{H,C}$ = 25 °C, and $T_{L,C}$ = 15 °C are shown in Fig. 2. The numerical predictions are in excellent agreement with the theoretical results, so the developed model is reliable for analyzing the performance of the integrated system.

2.5. Investigation basis

The element lengths of TEG and TEC ranging from 0.6 to 2.4 mm are considered to account for the influence of geometry on system performance. Two different boundary conditions at the hot surface of TEG, with one the Neumann condition (i.e. a temperature is given) and the other with the Dirichlet condition (i.e. a heat transfer rate is given), are considered. The geometric values of base case and the operating (boundary) conditions are shown in Tables 2 and

Table 2
Geometric size (base case) and material properties of thermoelectric elements.

Geometry of TEC1-12708 [28]
W = 1.4 mm
D = 1.4 mm
L = 1.2 mm
Material properties [29]
$k = (62605 - 277.7T + 0.4131T^2) \times 10^{-4}$ W m^{-1} K^{-1}
$\rho = (5112 + 163.4T + 0.6279T^2) \times 10^{-10}$ Ωm
$\alpha = (22224 + 930.6T - 0.9905T^2) \times 10^{-9}$ V K^{-1}

Table 3
Operating (boundary condition) conditions of study.

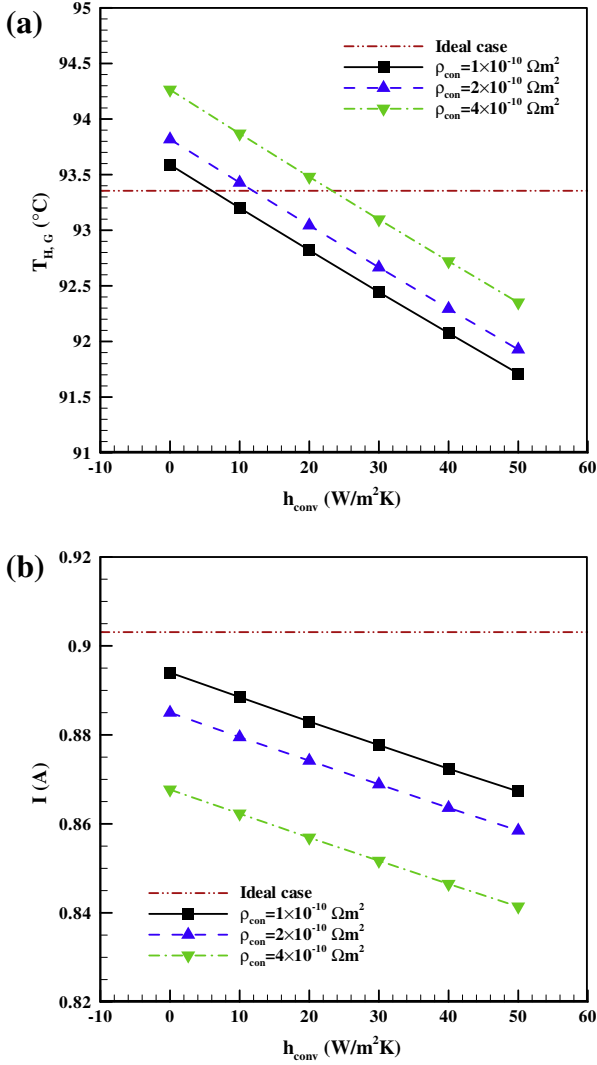| Surface	TEC	TEG
Hot side	Dirichlet condition: $T_{H,C}$ = 25 °C	Case1: Dirichlet condition: $T_{H,C}$ = 100 °C Case2: Neumann condition: $Q_{H,G}$ = 0.5 W
Cold side	Dirichlet condition: $T_{L,C}$ = 15 °C	Dirichlet condition: $T_{L,G}$ = 25 °C °C
Lateral side	Convection condition: h_{conv} = 20 W m^{-2} K^{-1} T_∞ = 25 °C	Convection condition h_{conv} = 20 W m^{-2} K^{-1} T_∞ = 25 °C

(a)

(b)

Fig. 3. Distributions of (a) hot surface temperature of the TEG and (b) electric current of the system (base case).
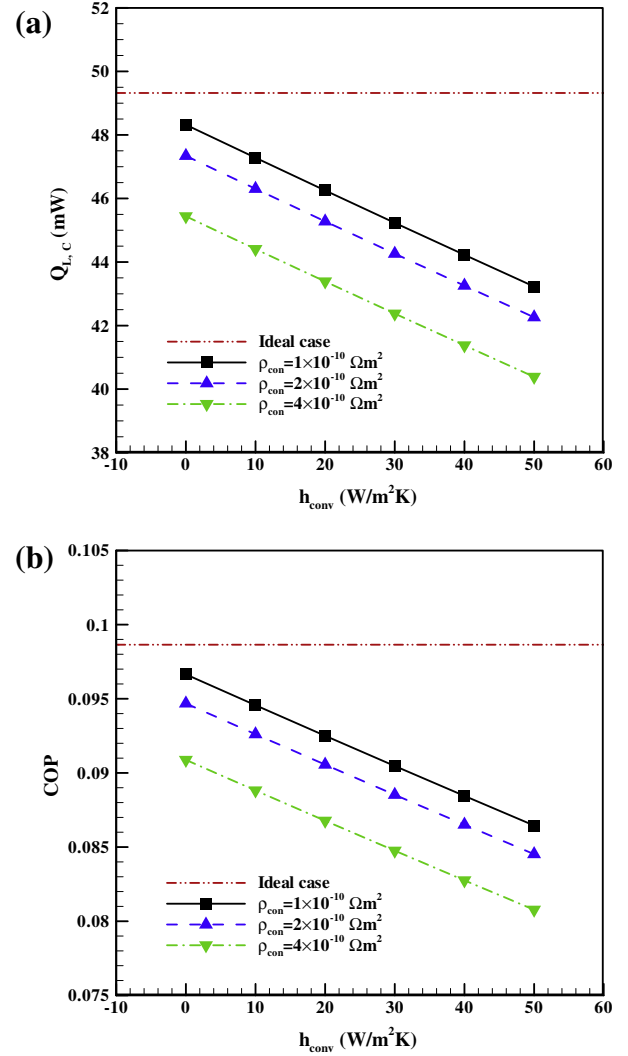
(a)

(b)

Fig. 4. Distributions of (a) cooling power and (b) COP (base case).

3, respectively. The solar thermoelectric generator, which uses concentrated solar radiation as a heat source, has received much attention lately [35]. The input energy (Q_{in}) of a thermal-concentrated solar thermoelectric generator can be represented by [36,37]

$$Q_{in} = q_s \times C_g \times A_c \times \eta_{opt} \times \eta_a \qquad (10)$$

where q_s, C_g, A_c, η_{opt}, and η_a are the solar irradiance, the concentration ratio, the cross-sectional area of the collector, the optical efficiency of the Fresnel lens, and the absorptivity of the collector coating, respectively. The cross-sectional area of the collector is assumed to be equivalent to the cross-sectional area of the thermoelectric module. With the conditions of q_s = 900 W m^{-2}, C_g = 50, η_{opt} = 85, and η_a = 0.9 [36] as well as A_c = 40 × 40 mm^2 for the thermoelectric module TEC1-12708 [28], the input energy is

$$Q_{in} = 900 \times 50 \times (40 \times 40 \times 10^{-6}) \times 0.85 \times 0.9 = 55.08 \text{ W} \qquad (11)$$

TEC1-12708 consists of 127 thermoelectric couples [28], so the input energy per couple (Q_{TE}) is Q_{TE} = 55.08/127 ≈ 0.43 W and this value is close to 0.5 W. For this reason, the boundary condition of $Q_{H,G}$ = 0.5 W is selected in this work. In addition, the maximum temperature of the TEG does not exceed the operating temperature limit of the thermoelectric module in all simulations with the

aforementioned boundary condition. The contact resistivity and convection heat transfer coefficient of the base case are set as 1×10^{-10} Ω m^{-2} [34] and 20 W m^{-2} K^{-1} [21,38], respectively.

3. Results and discussion

3.1. Influences of heat convection and contact resistance on system performance

The influences of convection heat transfer coefficient and contact resistivity on system performance at the condition of $Q_{H,G}$ = 0.5 W are shown in Figs. 3 and 4. The convection heat transfer coefficient and contact resistivity are in the ranges of 0–50 W m^{-2} K^{-1} [21,37] and 1×10^{-10}–4×10^{-10} Ω m^{-2} [18,34], respectively. The ideal case disregarding heat convection and contact resistance is also included for comparison. It can be seen that the hot surface temperature of the TEG rises with increasing ρ_{con} but decreases with h_{conv} (Fig. 3a). The energy balance at the TEG hot surface is expressed as [7,21]

$$Q_{H,G} = Q_{Pe} + Q_F - Q_J + Q_{conv,G} \qquad (12)$$

where Q_{Pe}, Q_F, Q_J, and $Q_{conv,G}$ designate the heat transfer rate due to the Peltier effect, Fourier conduction, Joule heating, and heat convection, respectively. The contact resistance can be conceived as an additional internal resistance of thermoelectric module [39];
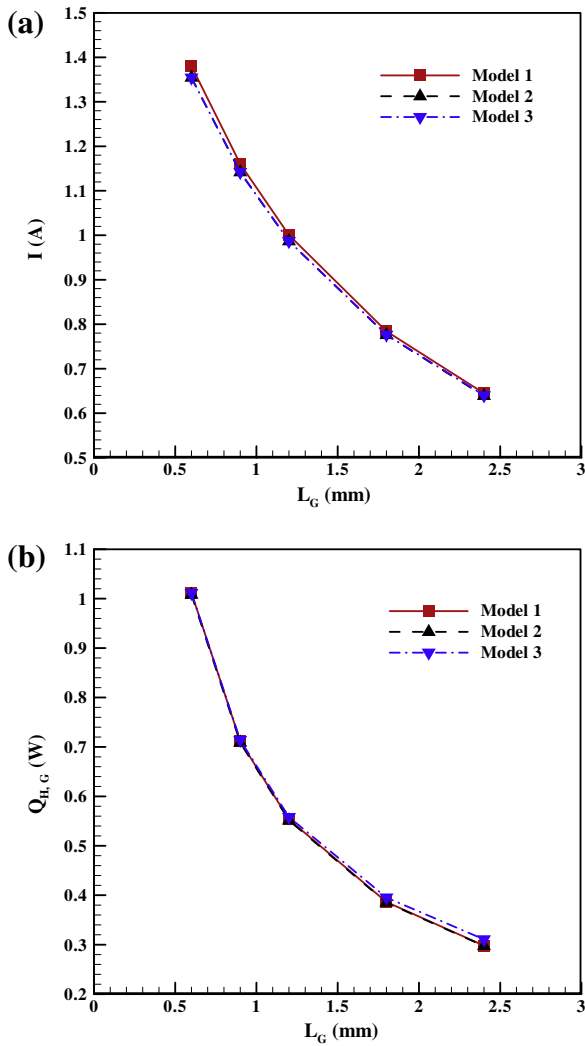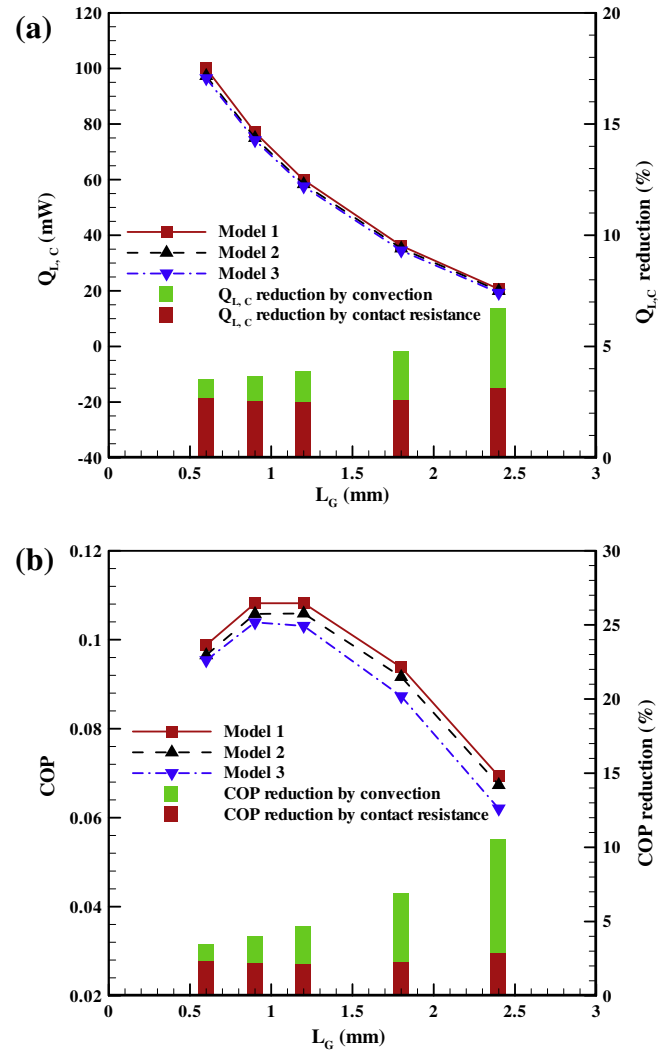
Fig. 5. Distributions of (a) electric current of the system and (b) heat input to the TEG ($T_{H,G}$ = 100 °C).

Fig. 6. Distributions of (a) cooling power and (b) COP and their reduction percentages ($T_{H,G}$ = 100 °C).

hence, an increase in ρ_{con} raises the Joule heat. In order to keep energy balance, the increased Joule heat may lead to the increase of Peltier heat (i.e., Eq. (12)). Accordingly, the hot surface temperature of the TEG increases because the Peltier heat at the hot surface is expressed as $Q_{Pe} = (\alpha_p - \alpha_n)IT_{H,G}$ [7,21]. Similarly, increasing convection heat transfer coefficient abates the Peltier heat due to the fixed $Q_{H,G}$, thereby decreasing the hot surface temperature of the TEG. The electric current of the integrated system diminishes as ρ_{con} goes up (Fig. 3b). This is attributed to the increased total resistance of the integrated system. The electric current also declines with increasing h_{conv}, and this reduces the cooling power (Fig. 4a). This is because the heat pumped at the TEC cold side through the Peltier effect (expressed as $(\alpha_p - \alpha_n)IT_{L,C}$ [30]) is the dominant mechanism [24]. A similar trend in COP under the condition of fixed $Q_{H,G}$ is also exhibited (Fig. 4b). Compared to the ideal case, the maximum reduction in cooling power (or COP) is 18.11% which occurs at $\rho_{con} = 4 \times 10^{-10}\ \Omega\,\mathrm{m}^{-2}$ and $h_{conv} = 50\ \mathrm{W\,m}^{-2}\,\mathrm{K}^{-1}$.

3.2. Influence of TEG element length at a given hot surface temperature of TEG

Two kinds of boundary condition at the hot surface of TEG are employed to analyze the influence of TEG element length on system performance. Meanwhile, three different models are regarded

for comparison: Model 1 (without contact resistance and heat convection), Model 2 (with contact resistance but without heat convection), and Model 3 (with both contact resistance and heat convection). With the condition of $T_{H,G}$ = 100 °C, the electric current of the integrated system decreases as the TEG length increases (Fig. 5a), resulting from the increased internal resistance of the TEG. This phenomenon can also be found from the theoretical formula of Khattab and Shenawy [12] (i.e., Eq. (9)). The decrease of electric current also abates the Peltier heat at the TEG hot surface. Therefore, $Q_{H,G}$ is lessened as the TEG element length increases (Fig. 5b). In Model 2, because the contact resistance increases the total resistance of the integrated system, the electric current of the system decreases (Fig. 5a). Furthermore, the decreased electric current and the increased resistance make the Joule heat become negligible. This is the reason why the heat input values of Model 2 are close to those of Model 1 (Fig. 5b). Seeing that the two surface temperatures of the TEG are fixed, the additional heat convection considered in Model 3 plays no part in changing the electric current when compared with Model 2 (Fig. 5a); however, a bit more heat input of $Q_{H,G}$ is required in Model 3.

The Peltier heat at the cold side of the TEC is the dominant mechanism of cooling power ($Q_{L,C}$) and it is proportional to the electric current; therefore, $Q_{L,C}$ decreases with increasing TEG length (Fig. 6a). When the effect of contact resistance on the
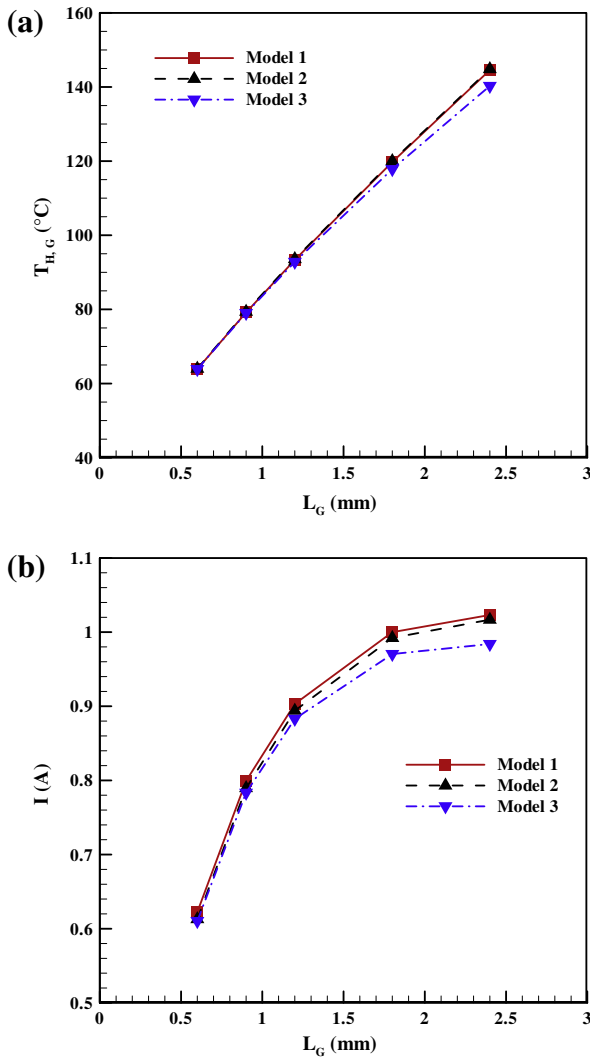
Fig. 7. Distributions of (a) hot surface temperature of TEG and (b) electric current of the system ($Q_{H,G}$ = 0.5 W).
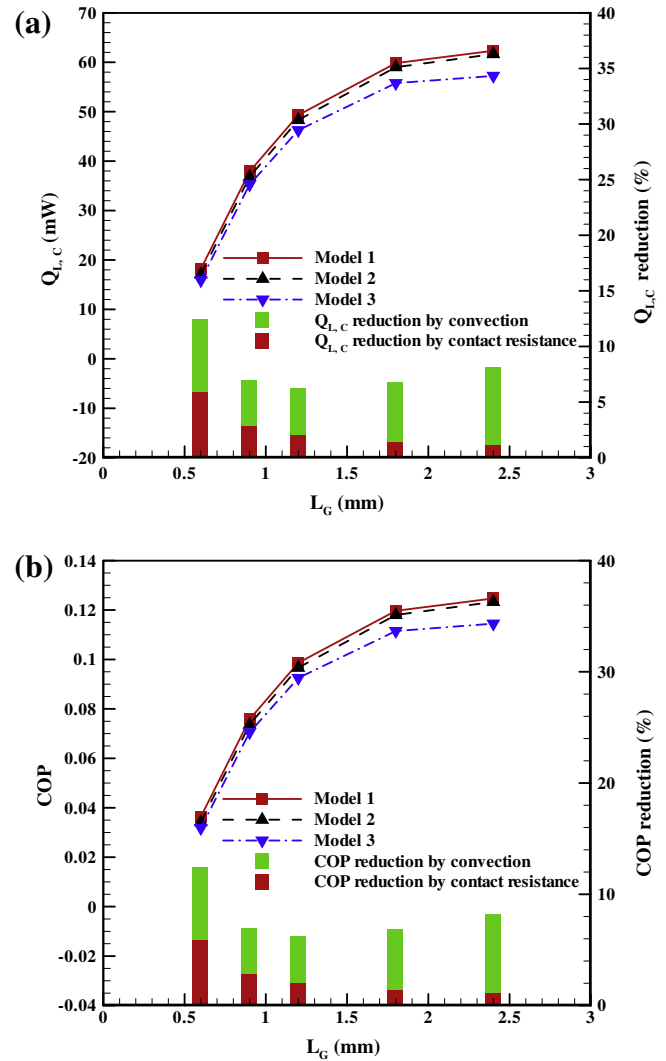

Fig. 8. Distributions of (a) cooling power and (b) COP and their reduction percentages ($Q_{H,G}$ = 0.5 W).

reduction percentage of $Q_{L,C}$ is examined, a minimum value develops at L_G = 1.8 mm. If both the heat convection and contact resistance are simultaneously considered, the maximum reduction percentage of $Q_{L,C}$ takes place at L_G = 2.4 mm. As a whole, both $Q_{H,G}$ and $Q_{L,C}$ are the decreasing functions of TEG element length (Figs. 5b and 6a). It is worthy of note that there exists an optimum L_G corresponding to the maximum COP (Fig. 6b). For example, the optimum TEG length in Model 3 is 0.9 mm. With regard to the reduction percentage of COP, Fig. 6b depicts that the effect of heat convection on COP tends to become more pronounced than that of contact resistance when the element length goes up. Within the investigated range of TEG length, the reduction percentage of COP is between 3.47% and 10.53%.

3.3. Influence of TEG element length at a given heat transfer rate of TEG

Figs. 7 and 8 demonstrate the system performance under a given heat transfer rate of $Q_{H,G}$ = 0.5 W at the hot surface of the TEG, whereas its cold surface temperature is fixed. Contrary to Fig. 5 in which the hot surface temperature is fixed, an increase in element length raises the TEG hot surface temperature

(Fig. 7a), stemming from the increased thermal resistance of the TEG [40]. In view of the enlarged temperature difference, the electric current of the system grows with increasing TEG element length. Eq. (9) also elucidates the preceding behavior. The electric current of the system increases slowly when the length is large to a certain extent (Fig. 7b). The output power of the TEG is 0.018 W when its hot-side temperature reaches about 145 °C. This power is very close to the experimental result of Niu et al. [20] where the TEG power was 0.0183 W at the same hot surface temperature. As illustrated earlier, the electric current directly affects the Peltier heat at the cold surface of the TEC; hence increasing TEG element length increases the cooling power and COP (Fig. 8) and their profiles are similar to those of electric current. It should be pointed out that the case of L_G = 2.4 mm along with $Q_{H,G}$ = 0.5 W gives the best performance of the system (Fig. 8), but the lowest performance is exhibited at the condition of $T_{H,G}$ = 100 °C (Fig. 6). With attention paid to the reduction percentages of cooling power and COP, Fig. 8 reveals that the reduction due to the contact resistance declines when the element length increases, and the impact of convection on the reduction of cooling power or COP is more than the contact resistance. This is the reason that the difference between the curves of Models 2 and 3 is more notable than that between Models 1 and 2. Overall, the reduction percentage of COP caused
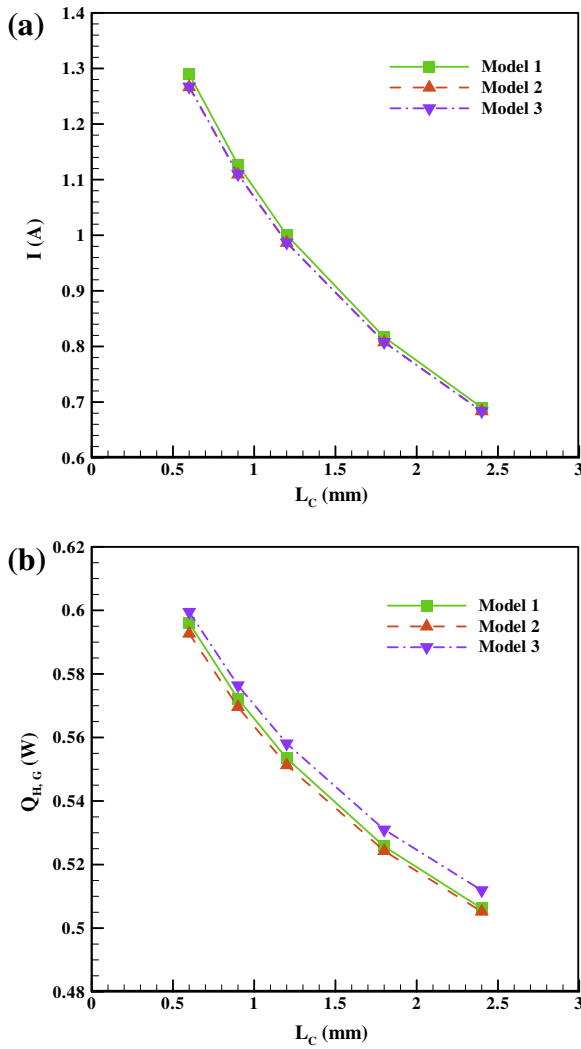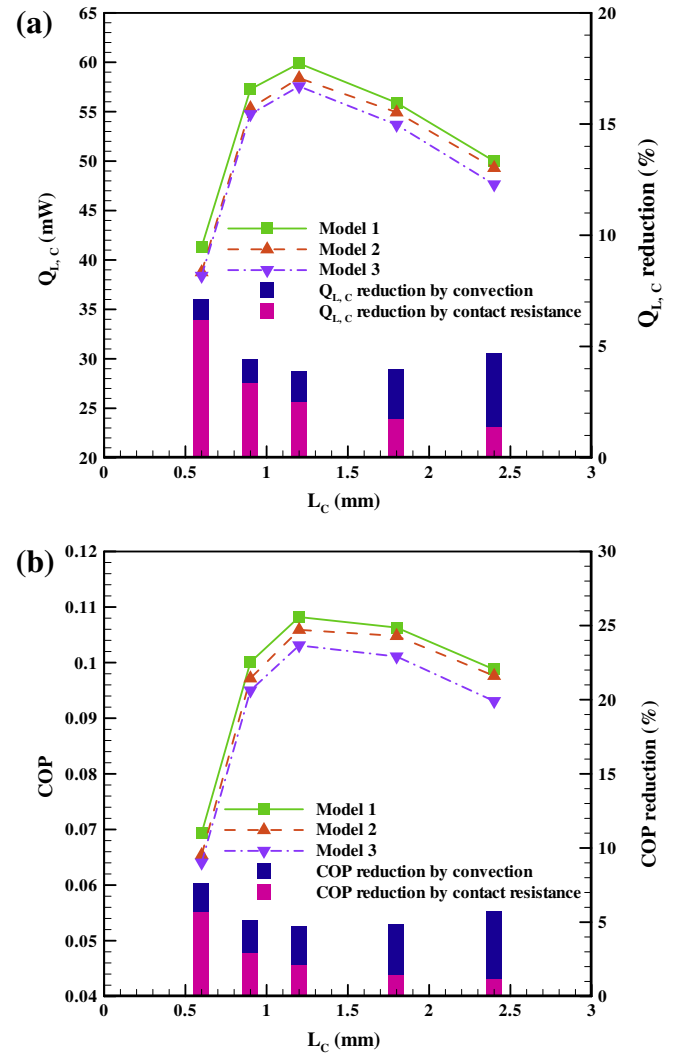
Fig. 9. Distributions (a) electric current of the system and (b) heat input to the TEG ($T_{H,G}$ = 100 °C).

Fig. 10. Distributions of (a) cooling power and (b) COP and their reduction percentages ($T_{H,G}$ = 100 °C).

by the heat convection and contact resistance is in the range of 6.22–12.45%.

3.4. Influence of TEC element length on system performance

The influence of TEC element length on system performance at the condition of $T_{H,G}$ = 100 °C is examined in Figs. 9 and 10 where the three different models are also included. The internal resistance of TEC increases when its element length rises, thereby diminishing the electric current of the system (Fig. 9a). This further lessens the Peltier heat at the TEG hot surface (i.e. $Q_{Pe} = (\alpha_p - \alpha_n)$-$IT_{H,G}$) so as to decrease the heat input into the TEG (Fig. 9b). It is worth noting that an optimum L_C corresponding to the maximum cooling power and COP can be identified (Fig. 10). For a shorter TEC, the importance of Peltier heat at the TEC cold surface precedes the Joule heat, as consequences of larger electric current and smaller internal resistance. However, heat diffusing back to the cold surface of the TEC by the Fourier conduction is pronounced because the total conductance of a thermoelectric couple is inversely proportional to the element length [14]. A lower cooling power is thus featured by a shorter TEC. When the TEC becomes taller, the Fourier conduction is weakened so the cooling power increases. When L_C is large to a certain extent, the Peltier heat

decreases because of smaller electric current. Once the Peltier heat is down to a level insufficient to counteract the Joule heat and Fourier conduction heat, the cooling power decreases. Unlike the behavior shown in Fig. 5b, there exist perceptible differences in $Q_{H,G}$ among the three curves shown in Fig. 9b, implying that the existences of contact resistance and convection affect the heat input to a small extent, especially for the latter where more heat inputted to the TEG is observed. In Fig. 10, the largest total reduction percentages of cooling power and COP are 7.10% and 7.65%, respectively, where the TEC length (L_C) is 0.6 mm.

Upon inspection of system performance at $Q_{H,G}$ = 0.5 W under the situation of varied TEC length, the electric current of the system decreases with increasing TEC length (Fig. 11a), resulting from the increased internal resistance of the TEC. Furthermore, the reduced current affects the energy balance at the TEG hot surface. On account of fixed $Q_{H,G}$ and in order to keep the energy balance at the TEG hot surface, the hot surface temperature of the TEG increases (Fig. 11b). However, the temperature variation versus the length is not as significant as that shown in Fig. 7a. It is also noted that the contact resistance lifts the TEG hot surface temperature. The characteristics of the maximum cooling power and COP are observed in Fig. 12 where the optimum TEC length is 1.8 mm. The foregoing results are similar to those with fixed $T_{H,G}$ (Fig. 10).
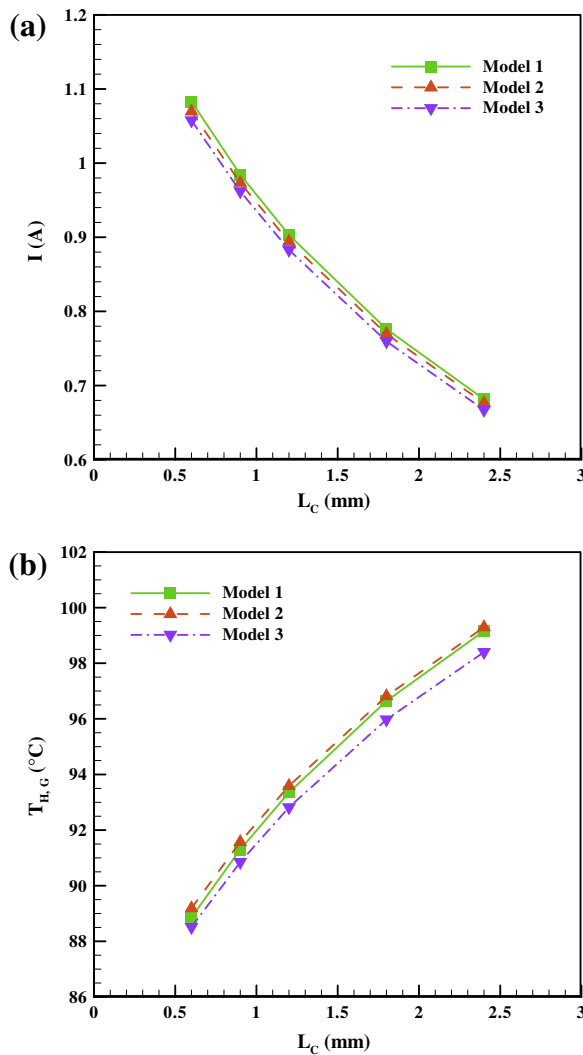
Fig. 11. Distributions of (a) electric current of the system and (b) hot surface temperature of the TEG ($Q_{H,G}$ = 0.5 W).

Fig. 12. Distributions of (a) cooling power and (b) COP and their reduction percentages ($Q_{H,G}$ = 0.5 W).

This can be explained by the same trend in electric current, even though the boundary conditions at the TEG hot surface are different from each other. The negative effects of contact resistance and heat convection on system performance can be found in Figs. 11 and 12. The largest total reduction percentages of cooling power and COP are obtained at L_C = 0.6 mm where their values are the same as 18.67%.

The characteristics of cooling power and COP in Model 3 in accordance with the selection of boundary condition and the variation of TEG or TEC length are summarized in Table 4. Apparently, the characteristics of cooling power and COP under the condition of varying TEG length are fairly different from those of varying TEC length. The boundary conditions play an important role in determining the system performance when the TEG length is altered, whereas an optimum TEC length can be obtained, regardless of the Dirichlet or Neumann condition adopted. Overall, the predictions reveal that the cooling power of the TEC is in the range of approximately 10–100 mW, which is by far smaller than the requirement of practical application. Accordingly, a feasible way for the application of the integrated system is that a TEC can couple with a number of TEGs in series to intensify the cooling power of the TEC. The aforementioned system deserves further investigation in the future.
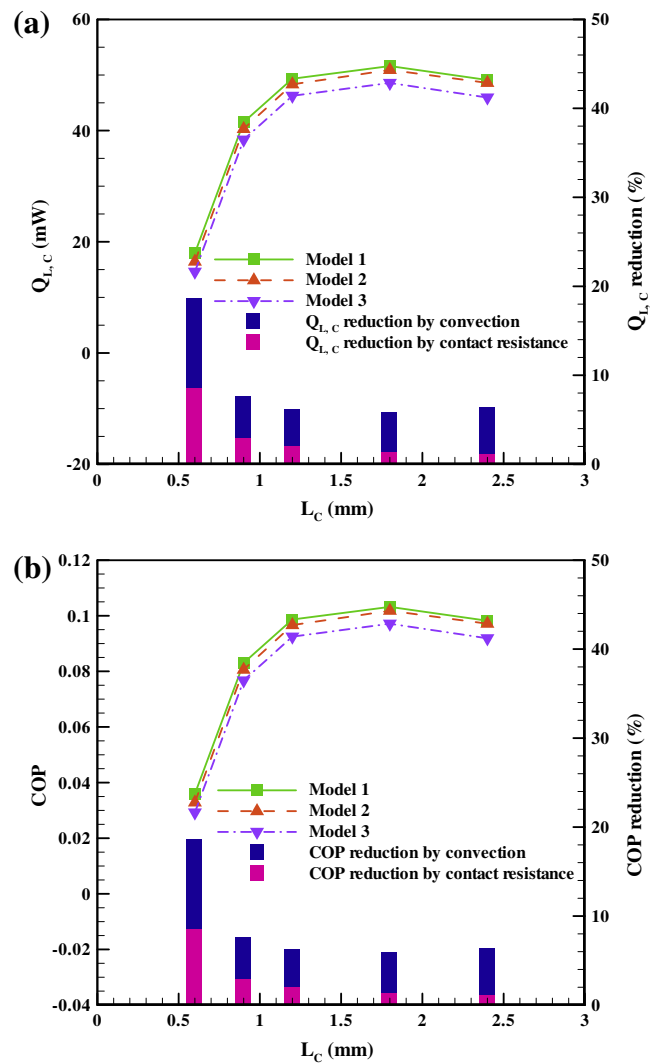
Table 4
Summary of system performance of Model 3 at various operating conditions.

	Cooling power	COP
Increasing TEG length		
Dirichlet condition[a]	Decrease	Optimum at L_G = 0.9 mm
Neumann condition[b]	Increase	Increase
Increasing TEC length		
Dirichlet condition[a]	Optimum at L_C = 1.2 mm	Optimum at L_C = 1.2 mm
Neumann condition[b]	Optimum at L_C = 1.8 mm	Optimum at L_C = 1.8 mm

[a] $T_{H,G}$ = 100 °C.
[b] $Q_{H,G}$ = 0.5 W.

4. Conclusions

The physical phenomena of an integrated TEG–TEC system have been analyzed through a numerical method. Particular attention is paid to the influences of geometric sizes of TEG and TEC and boundary conditions upon the performance of the integrated system. The effects of contact resistance and heat convection on the performance have also been examined. The predictions suggest that the cooling power and coefficient of performance (COP) of the system are reduced when the contact resistance and heat convection are taken into account. For a given hot surface temperature

of TEG, the higher the TEG length, the larger the reduction percentages of cooling power and COP. For the other cases, an optimum length for minimizing the reduction percentage can be found. However, the minimum reduction percentage does not always respond to the maximum system performance. When the lengths of TEG and TEC are individually altered, the system performances are reduced up to 12.45% and 18.67%, respectively. Considering the impacts of geometric size and boundary conditions on the performance, the cooling power and COP of the system are significantly affected by the boundary conditions when the TEG length is changed. In contrast, an optimum length corresponding to the maximum cooling power and COP is exhibited if the TEC length is varied, irrespective of whether the boundary condition of fixed temperature (Dirichlet) or heat transfer rate (Neumann) is given. The predictions suggest that the cooling power of the TEC in the integrated system is in the range of approximately 10–100 mW. These values are fairly small for practical applications. A feasible way for the application of the integrated system is the coupling of a TEC with a number of TEGs in series to intensify the cooling power of the TEC. The present study has provided a useful insight into the design of integrated TEG-TEC systems which enables us to refrigerate an object by using waste heat as a power source.

Acknowledgment

References

[1] Ahiska R, Mamur H. A test system and supervisory control and data acquisition application with programmable logic controller for thermoelectric generators. Energy Convers Manage 2012;64:15–22.

[2] Meng JH, Wang XD, Zhang XX. Transient modeling and dynamics characteristics of thermoelectric cooler. Appl Energy 2013;108:340–8.

[3] Karabetoglu S, Sisman A, Ozturk ZF, Sahin T. Characterization of a thermoelectric generator at low temperatures. Energy Convers Manage 2012;62:47–50.

[4] Chen WH, Chiu TW, Hung CI. Hydrogen production from methane under the interaction of catalytic partial oxidation, water gas shift reaction and heat recovery. Int J Hydrogen Energy 2010;35:12808–20.

[5] Chen WH, Syu YJ. Thermal behavior and hydrogen production of methanol autothermal reforming with spiral preheating. Int J Hydrogen Energy 2012;36:3397–408.

[6] Wang XD, Huang YX, Cheng CH, Lin DTW. A three-dimensional numerical modeling of thermoelectric device with consideration of coupling of temperature field and electric potential field. Energy 2012;47:488–97.

[7] Meng F, Chen L, Sun F. A numerical model and comparative investigation of a thermoelectric generator with multi-irreversibilities. Energy 2011;36:3513–22.

[8] Yu C, Chau KT. Thermoelectric automotive waste heat energy recovery using maximum power point tracking. Energy Convers Manage 2009;50:1506–12.

[9] Chen WH, Liao CY, Hung CI, Haung WL. Experimental study on thermoelectric modules for power generation at various operating conditions. Energy 2012;45:874–81.

[10] Lertsatitthanakorn C, Wiset L, Atthajariyakul S. Evaluation of the thermal comfort of a thermoelectric ceiling cooling panel (TE-CCP) system. J Electron Mater 2009;38:1472–7.

[11] Chen X, Lin B, Chen J. The parametric optimum design of a new combined system of semiconductor thermoelectric devices. Appl Energy 2006;83:681–6.

[12] Khattab NM, Shenawy ETE. Optimal operation of thermoelectric cooler driven by solar thermoelectric generator. Energy Convers Manage 2006;47:407–26.

[13] Meng F, Chen L, Sun F, Wu C. Thermodynamic analysis and optimization of a new-type thermoelectric heat pump driven by a thermoelectric generator. Int J Ambient Energy 2009;30:95–101.

[14] Meng F, Chen L, Sun F. Multiobjective analysis of physical dimension on the performance. Int J Low-Carbon Technol 2010;5:193–200.

[15] Sahin AZ, Yilbas BS. The thermoelement as thermoelectric power generator: effect of leg geometry on the efficiency and power generation. Energy Convers Manage 2014;78:634–40.

[16] Jang B, Han S, Kim JY. Optimal design for micro-thermoelectric generators using finite element analysis. Microelectron Eng 2011;88:775–8.

[17] Lee KH, Kim OJ. Analysis on the cooling performance of the thermoelectric micro-cooler. Int J Heat Mass Transfer 2007;50:1982–92.

[18] Sharp J, Bierschenk J, Lyon JHB. Overview of solid-state thermoelectric refrigerators and possible applications to on-chip thermal management. Proc IEEE 2006;94:1602–12.

[19] Min G, Rowe DM. Improved model for calculating the coefficient of performance of a Peltier module. Energy Convers Manage 2000;41:163–71.

[20] Niu X, Yu J, Wang S. Experimental study on low-temperature waste heat thermoelectric generator. J Power Sources 2009;188:621–6.

[21] Xiao H, Gou X, Yang S. Detailed modeling and irreversible transfer process analysis of a multi-element thermoelectric generator system. J Electron Mater 2011;40:1195–201.

[22] Bell LE. Cooling, heating, generating power, and recovering waste heat with thermoelectric systems. Science 2008;321:1457–61.

[23] Chatterjee S, Pandey KG. Thermoelectric cold-chain chests for storing/transporting vaccines in remote regions. Appl Energy 2003;76:415–33.

[24] Chen WH, Liao CY, Hung CI. A numerical study on the performance of miniature thermoelectric cooler affected by Thomson effect. Appl Energy 2012;89:464–73.

[25] Wang CC, Hung CI, Chen WH. Design of heat sink for improving the performance of thermoelectric generator using two-stage optimization. Energy 2012;39:236–45.

[26] Moaveni S. Finite element analysis: theory and applications with ANSYS. 2nd ed. New Jersey: Prentice Hall; 2003.

[27] Antonova EE, Looman DC. Finite elements for thermoelectric device analysis in ANSYS. In: 24th Int. conference on thermoelectrics; 2005: 200.

[28] Maneewan S, Chindaruksa S. Thermoelectric power generation system using waste heat from biomass drying. J Electron Mater 2009;38:974–80.

[29] Meng F, Chen L, Sun F. Effects of temperature dependence of thermoelectric properties on the power and efficiency of a multielement thermoelectric generator. Int J Energy Environ 2012;3:137–50.

[30] Pérez-Aparicio JL, Palma R, Taylor RL. Finite element analysis and material sensitivity of Peltier thermoelectric cells coolers. Int J Heat Mass Transfer 2012;55:1363–74.

[31] Gou X, Xiao H, Yang S. Modeling, experimental study and optimization on low-temperature waste heat thermoelectric generator system. Appl Energy 2010;87:3131–6.

[32] Hsu CT, Yao DJ, Ye KJ, Yu B. Renewable energy of waste heat recovery system for automobiles. J Renew Sustain Energy 2010;2:013105.

[33] Champier D, Bédécarrats JP, Kousksou T, Rivaletto M, Strub F, Pignolet P. Study of a TE(thermoelectric) generator incorporated in a multifunction wood stove. Energy 2011;36:1518–26.

[34] Astrain D, Vian JG, Martinez A, Rodriguez A. Study of the influence of heat exchangers' thermal resistances on a thermoelectric generation system. Energy 2010;35:602–10.

[35] Xiao J, Yang T, Li P, Zhai P, Zhang Q. Thermal design and management for performance optimization of solar thermoelectric generator. Appl Energy 2012;93:33–8.

[36] Li P, Cai L, Zhai P, Tang X, Zhang Q, Niino M. Design of a concentration solar thermoelectric generator. J Electron Mater 2010;39:1522–30.

[37] Chen WH, Wang CC, Hung CI, Yang CC, Juang RC. Modeling and simulation for the design of thermal-concentrated solar thermoelectric generator. Energy 2014;64:287–97.

[38] Chen M, Rosendahl LA, Condra T. A three-dimensional numerical model of thermoelectric generators in fluid power systems. Int J Heat Mass Transfer 2011;54:345–55.

[39] Liang G, Zhou J, Huang X. Analytical model of parallel thermoelectric generator. Appl Energy 2011;88:5193–9.

[40] Cheng CH, Huang SY, Cheng TC. A three-dimensional theoretical model for predicting transient thermal behavior of thermoelectric coolers. Int J Heat Mass Transfer 2010;53:2001–11.